JOURNAL OF CATALYSIS 152, 252–263 (1995)

Pt-Black Catalysts Sintered at Different Temperatures: Surface Analysis and Activity in Reactions of *n*-Hexane

Zoltán Paál,*,†,[1] Xian Lun Xu,*,[2] Julia Paál-Lukács,* Walter Vogel,† Martin Muhler,† and Robert Schlögl†

*Institute of Isotopes of the Hungarian Academy of Sciences, P.O. Box 77, H-1525 Budapest, Hungary; and †Fritz-Haber-Institut der Max-Planck-Gesellschaft, Faradayweg 4/6, D-14195 Berlin (Dahlem), Germany

Pt-black catalysts sintered at 473 and 633 K ("Pt-473" and "Pt-633"), respectively, have been characterized by X-ray diffraction and analyzed by XPS, UPS, and AES after carrying out *n*-hexane reactions. The analysis has been repeated after O_2–H_2 regeneration in the preparation chamber of the UHV apparatus. The surface of the blacks contains some carbon and oxygen impurities even after regeneration. Both Pt-473 and Pt-633 show high Pt 4*f* line intensity. Decomposition of the C 1*s* line reveals a higher amount of oxidized carbon polymers on Pt-633. This sample is free from lattice strain. The likely higher abundance of exposed hexagonal symmetry faces, namely the (111) plane and analogous stepped and kinked structures, may be one of the reasons why fragmentation and aromatization are favored on Pt-633, as opposed to the higher selectivity of isomerization and C_5-cyclization on Pt-473. The higher amount of oxidized carbonaceous polymer overlayer (serving as "hydrogen catcher") on Pt-633 as well as the less-retained hydrogen by its crystallites without lattice strain may also contribute to the different selectivity and hydrogen pressure response of the *n*-hexane reaction over the two samples. Product ratios are suggested as an additional diagnostic tool for characterizing the hydrogen availability on the catalysts. © 1995 Academic Press, Inc.

INTRODUCTION

Heating Pt-black between 470 and 650 K in hydrogen induces sintering, producing aggregates consisting of individual crystallites with various sizes (1). Hydrogen may penetrate into subsurface layers even around 300 K and decrease the lattice strain of dispersed Pt crystallites (2). The temperature of the first contact of Pt-black with hydrogen is decisive with respect to the final average crystallite size (1). Electron microscopy of these samples (1, 3) permitted us to estimate crystallite sizes and also revealed that the shape of Pt grains is rounded. Hence, varying amounts of crystal planes with different, not always low, Miller indices will be exposed after this primary, hydrogen-induced recrystallization. Preliminary results of XPS and Auger analysis (3, 4) indicated that all Pt-black samples contained carbonaceous and oxygenated impurities. Their abundance, location (as a result of their migration during sintering), and chemical form may influence the catalytic properties.

Portions of the same batch of Pt-black have been sintered in H_2 at two different temperatures: 473 and 633 K. These catalysts showed different activities and selectivities in the transformations of five *n*-heptane isomers at constant hydrocarbon pressure and constant sampling time (3). The absolute yields were, as a rule, higher over Pt-473, but higher aromatic yields could be achieved over Pt-633. The hydrogen response of reactions over these two samples was also different: maximum yields were typical as a function of $p(H_2)$ with Pt-633, rather than a monotonic increase of yields observed for Pt-473. The possible reasons for the different catalytic properties have been discussed together with a detailed survey of literature suggestions (3).

The present study reports on physical characterization and further catalytic testing with *n*-hexane as the probe molecule for the same Pt-473 and Pt-633 samples as described previously (3). X-ray diffraction and electron spectroscopic measurements were added to earlier electron microscopic studies (3) as methods of physical catalyst characterization. Detailed evaluation of electron spectra of Pt-black samples from the surface science point of view and a comparison with relevant literature data has been reported elsewhere (5–7). We hope that the evaluation of physical characterization together with catalytic testing may provide information on the possible active sites and may reveal reasons why the catalytic properties of the two samples are different.

The present study continues previous ones on the catalytic properties of different Pt catalysts in model reactions (3, 8, 9). Two related papers (10, 11) also contain electron spectra and catalytic properties of fresh Pt-black samples of different preparation.

[1] To whom correspondence should be addressed.

[2] On leave from Lanzhou Institute of Physical Chemistry, Academia Sinica, Lanzhou, P. R. China.

0021-9517/95 $6.00

EXPERIMENTAL

Sample preparation and pretreatment. Pt-black catalysts were prepared by reduction of H_2PtCl_6 by the aqueous solution of HCHO in the presence of KOH (3) and were presintered in hydrogen at 473 and 633 K, respectively. The same 100-mg batches were used as in Ref. (3). The present samples were measured after several dozens of catalytic runs, typically at 600 K (duration between 1 and 100 min) also involving the same number of regenerations with O_2 and H_2.

Catalytic runs. A closed circulation loop glass reactor was used for catalytic testing at 603 K (12, 13). Runs were carried out at two *n*-hexane (nH) pressures (1.33 and 5.33 kPa) and two hydrogen pressures (16 and 64 kPa). Samples were taken after different times (1 to ca. 100 minutes) and analyzed by a 50 m × 0.32 mm fused quartz capillary column (coated with CP Sil 5) under isothermal conditions, ensuring a proper separation from methane to benzene.

X-ray diffraction. The details of X-ray diffraction measurements have been described earlier (14, 15). Briefly, high-resolution X-ray diffraction patterns of Pt-473 and Pt-633 taken out from the catalytic reactor, as well as that of their unsintered precursor, were measured under ambient atmosphere with a commercial Guinier diffractometer (Huber) in the 45° transmission geometry. The system was equipped with a Johansson-type Ge monochromator to produce a focused Cu$K\alpha_1$ primary beam. Samples were prepared by sieving the powders on a 3-μm polyethylene foil using a Uhu-acetone adhesive. A blank sample was used for background correction. Correction of the line profiles for instrumental broadening could be neglected in the present setup.

Electron spectroscopy. An analysis chamber equipped with sources for X-ray photoelectron spectroscopy (XPS), ultraviolet photoelectron spectroscopy (UPS) and Auger-electron spectroscopy (AES), and a Leybold EA-12 hemispherical analyzer was used. Spectra were processed with Leybold DS-100 software; functions for smoothing, background subtraction, peak integration, and line fitting were utilized. Additional fitting procedures were also carried out with the SciPlot[C] program developed by M. Wesemann. Pt 4*f*, C 1*s*, K 2*p*, and O 1*s* lines of the XPS were monitored (Mg$K\alpha$ anode, pass energy, 50 eV). Integral Auger electron spectra obtained with 5 kV excitation voltage were differentiated by the Leybold DS-100 software and the peak-to-peak distances of the lines at 1967 eV for Pt, 503 eV for 0, 270 eV for C, and 252 eV for K were used. The formula given in Ref. (16) and the atomic sensitivity factors plotted in the same reference were used for quantitative evaluation. He I UP spectra were measured with a pass energy of 4 eV. Difference spectra produced by subtracting two individual spectra (directly or after intensity normalization) are also shown. Raw, smoothed, and fitted spectra, in most cases after background subtraction, are included in the present study.

Line fitting to XP spectra: possibilities and limitations. Whenever the regions were decomposed to individual components (in the O 1*s* and C 1*s* regions), symmetric lines with the same Gaussian-to-Lorentzian mixing ratio were used after Shirley-type background subtraction. The self-consistency principle has been utilized in fitting individual components (5): the fwhm values of individual components have been fixed according to literature values (5) and the program itself found the BE maxima. The consistency required sometimes to include some low-intensity lines, for example, the line at BE 534 eV in the O 1*s* band (Fig. 5) or adding the line at a fixed BE of 283.3 eV in the C 1*s* band (Fig. 6). Concentrations of individual components calculated with windows of different width and using raw or smoothed spectra agreed within ±15%. A larger uncertainty is natural at the highest- and lowest-energy edges of the bands where the signal-to-noise ratio is poorer. These values present not more but not less than fair semiquantitative information on the abundance of the respective components.

RESULTS

Catalytic Reactions of n-Hexane

Activity. Plotting yields (Y) as a function of overall conversion (X) [$Y - X$ plots or optimum performance envelopes (17)] are informative on the possible primary and secondary products. Primary products have finite slope near-to-zero conversion; secondary products have zero slope. Decreasing slopes denote consumption of the product in secondary reactions, whereas increasing slope means product accumulation in more than one reaction.

Yield vs conversion ($Y - X$) plots shown in Fig. 1 use Pt-633 as an example illustrating the hydrocarbon pressure dependence. Straight lines are characteristic of most $Y - X$ plots. Increasing $p(n\mathrm{H})$ by four times brought about hardly any changes at $p(H_2)$ = 16 kPa, its effect being just visible with hydrogenolysis, hexene formation, and isomerization. Aromatization has the second highest yield at this low hydrogen excess (Fig. 1a); this reaction as well as C_5-cyclization is independent of *n*-hexane pressure. Olefins (straight-chain hexene isomers) accumulate initially, but their amount increases very slowly above 2–3% conversion at $p(H_2)$ = 16 kPa.

Similar curves measured at a higher hydrogen excess (1.33 : 64) are compared in Fig. 2 for both catalysts. Aromatization is suppressed at this higher $p(H_2)$ (Fig. 2a). A

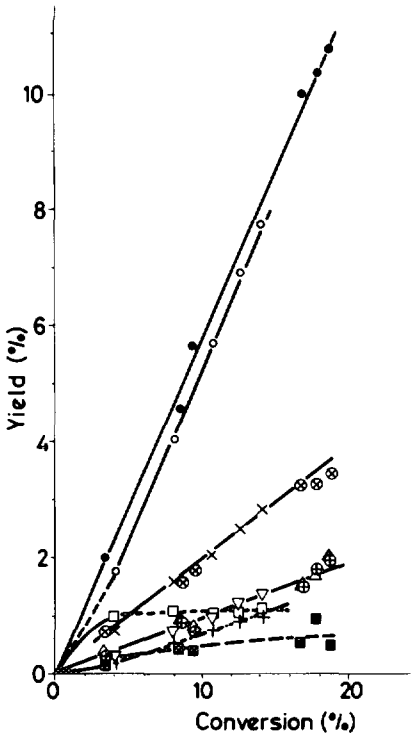

FIG. 1. Yields of individual products from *n*-hexane over Pt-633 as a function of the overall conversion at 603 K at $p(H_2)$ = 16 kPa and two different *n*-hexane pressures. $p(nH)$ = 1.33 kPa: (●) $<C_6$ fragments; (⊕) isomers; (△) methylcyclopentane; (■) olefins; (⊗) benzene. $p(nH)$ = 5.33 kPa: (○) $<C_6$ fragments; (+) isomers; (▽) methylcyclopentane; (□) olefins; (×) benzene.

short "running-in" period (i.e., a positive deviation from linearity) is seen for hydrogenolysis. Isomerization is affected most spectacularly by the higher hydrogen pressure; isomers belonging to the most abundant products at $p(H_2)$ = 64 kPa and the increasing slope of the isomerization yield between 0 and 2% conversion indicates that they are secondary products. As opposed to low hydrogen excess (Fig. 1), the consumption of methylcyclopentane (MCP) can be observed at higher conversion values at $p(H_2)$ = 64 kPa. The role of hexenes is negligible at this H_2 pressure.

The curves for Pt-473 (Fig. 2b) correspond to lower conversions than those obtained with Pt-633 in Fig. 1b. Hydrogenolysis is *not* the main reaction over the catalyst, as isomerization exceeds its yield over 4% conversion. Despite their different relative positions, the *shape* of the respective curves resembles that observed with Pt-633.

Selectivity. Plotting selectivities as a function of the conversion (*S-X* plots) is another useful tool to distinguish between primary and secondary products (18). A product with zero selectivity at zero conversion seems to be a secondary one whereas a primary product leads to a finite intersection of the ordinate. This is shown in Fig. 3 for Pt-473 and Pt-633 at the highest (1.33 : 64) and lowest (5.33 : 16) hydrogen excess. The primary character of benzene, fragments and olefins over Pt-473, is clearly seen; having no results at $X < 4\%$, this cannot be stated with certainty for aromatization over Pt-633. Very different hydrogenolysis and isomerization selectivities are observed with the two catalysts at both hydrogen pressures while the olefin selectivities are very close to each other. Hydrogenolysis and aromatic selectivity is lower, while that of isomers and methylcyclopentane is higher over Pt-473 than over Pt-633.

Three parameters for *hydrogenolysis* are shown in Table 1. The value of ζ (19) indicates the number of fragments per decomposed parent molecule. This value is just over 2 (except for it reaching almost 4 in one case) indicating a basically single hydrogenolysis with some superimposed multiple fragmentation over both catalysts. The parameter M_f relates the amount of $>C_2$ fragments to that of methane (20). With $M_f > 1$, random or internal hydrogenolysis occurs, while $M_f = 1$ means a repeated terminal splitting producing much methane. The values of M_f are lower over Pt-633, in agreement with the higher methane excess over this catalyst. Unlike ζ, M_f exhibits a hydrogen pressure dependence which is different for the two catalysts: highest M_f values are seen at intermediate $p(H_2)$ over Pt-633 and at low $p(H_2)$ over Pt-473. Finally, ω shows the chances of single rupture in various positions related to purely random breakup (21). The values calcu-

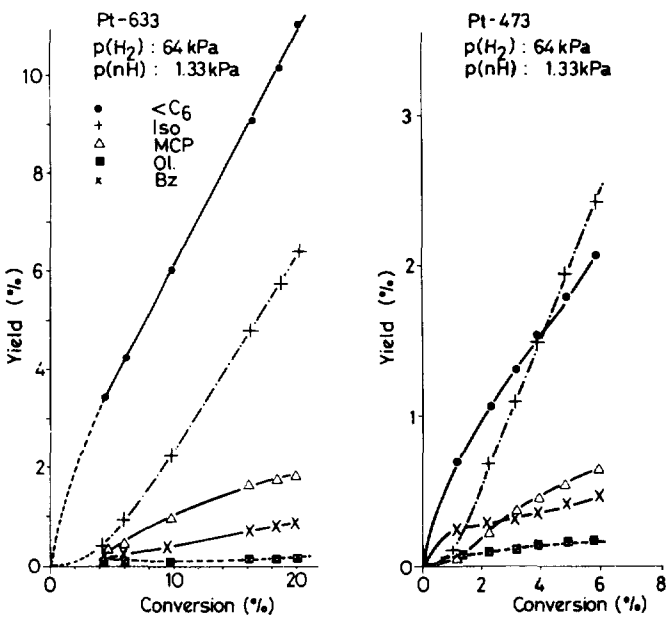

FIG. 2. Yields of individual products from *n*-hexane over Pt-633 and Pt-473 as a function of the overall conversion; at $p(H_2)$ = 64 kPa, $p(nH)$ = 1.33 kPa at 603 K.

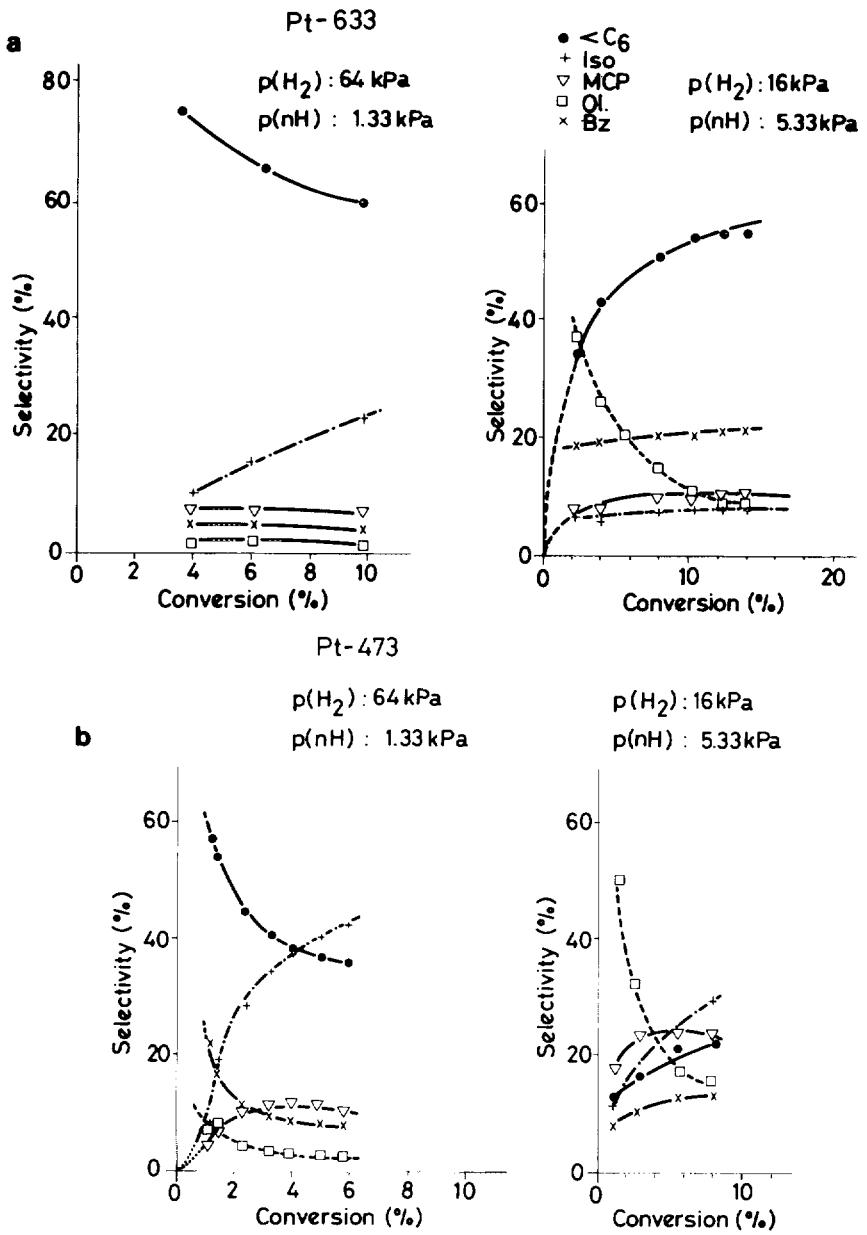

FIG. 3. Selectivities of individual products for *n*-hexane as a function of the overall conversion at two $p(n\mathrm{H}):p(\mathrm{H_2})$ ratios (1.33 : 64 and 5.33 : 16) at 603 K. (a) Pt-633; (b) Pt-473.

lated from the larger fragment (e.g., only C_4 is considered to calculate ω_2 with a breakdown $C_6 \rightarrow C_2 + C_4$; similarly, C_3 is used to calculate ω_3 and C_5 for ω_1) indicate a strong preference of splitting in the middle of the *n*-hexane molecule. Considerable terminal rupture is seen over Pt-633 at low hydrogen pressures only.

X-Ray Diffraction

Electron microscopy showed that both catalyst samples consisted of an agglomeration of smaller crystallites, the size of individual grains being markedly higher with Pt-633. This is confirmed by the X-ray diffraction analysis (Table 2). Rather high stacking fault probability is seen with the unsintered Pt-black, where also the internal lattice stress is pronounced, exceeding more than five times the value of 180 N/mm^2 reported for an untreated Pt/SiO_2 catalyst with a crystallite size of 17.5 nm (15). Sintering in hydrogen at higher and higher temperatures brings about not only crystallite size growth (as indicated by particle sizes and X-ray dispersion in Table 2), but also considerably decreases the internal lattice stress, and the

TABLE 1

Characteristics of *n*-Hexane Hydrogenolysis at Different Conversions

Sample	$p(H_2)$ (kPa)	$p(nH)$ (kPa)	X (%)[a]	ζ[b]	M_f[c]	ω_1[d]	ω_2[d]	ω_3[d]	CH_4 (%)[e]
Pt-633	16	5.33	4.0	2.34	2.57	1.36	0.42	1.22	45
			14.1	2.28	2.68	1.51	0.46	1.03	44
	16	1.33	3.5	2.20	4.99	0.73	0.65	1.62	35
			16.8	2.14	3.84	1.18	0.48	1.33	39
	64	1.33	4.4	3.92	1.49	0.36	0.55	2.09	69
			16.4	2.52	4.97	0.46	0.68	1.86	36
Pt-473	16	5.33	3.6	2.21	7.44	0.50	0.66	1.84	27
			8.2	2.26	6.91	0.53	0.68	1.79	28
	16	1.33	5.2	2.29	7.35	0.44	0.68	1.88	27
			8.8	2.28	7.52	0.42	0.70	1.88	27
	64	1.33	3.2	2.75	3.32	0.48	0.69	1.82	46
			5.7	2.50	4.28	0.59	0.67	1.74	39

[a] Conversion.
[b] $\zeta = (\Sigma C_i/\Sigma i/nC_i)$ (Ref. 19).
[c] $M_f = (\Sigma(n - i)C_i/C_1)$ (Ref. 20).
[d] ω = rate of actual rupture in a given position/rate of random rupture in the same position (Ref. 21); ω_1 calculated from the *n*-pentane; ω_2 from the *n*-butane and ω_3 from the propane fragment.
[e] Methane percentage calculated for $\Sigma < C_6 = 100\%$.

stacking fault probability, in agreement with previous results (2). The marked anisotropy in unsintered catalysts may bring about anisotropic deformations. This decreases considerably after sintering at 473 K and becomes zero with Pt-633. This sample represents a much more stabilized solid material with spherical symmetry, practically free from internal stress.

Electron Spectroscopy

Surface concentrations. Pt-black samples were subjected to electron spectroscopic analysis in two states: after transferring them from the reactor to the UHV apparatus in air ("as received" samples) and after applying a standard purification procedure ("regenerated" samples) analogous to standard catalyst regeneration between runs. The regeneration consisted of a treatment with 26 mbar O_2 for 3 min followed by a 5 min evacuation and 263 mbar H_2 for 10 min at 603 K in the preparation chamber.

Table 3 summarizes the surface compositions calculated from both XPS and AES. The escape depth of the Pt signal of 1967 eV is different from that for the kinetic energy of the Pt 4*f* XPS line (ca. 1180 eV), and this may represent one of the reasons for the higher Pt intensity measured. Another likely reason for the different composition may be that the high energy exciting electron beam of AES concentrated on a small area (ca. 2 mm^2 as opposed to ca. 30 mm^2 for XPS) may have caused local desorption of some adspecies, above all, that of oxygenated ones (Table 3). Carbon concentrations measured by XPS and AES are much closer to each other. Some surface water has been removed and as K_2CO_3 and/or KOH showed a relative surface enrichment. This latter result is in agreement with the high-intensity PtK^+ SIMS ion intensity of these catalysts (22). Since no Si signal was detected by XPS, the poorly reproducible low-intensity Si AES peaks reported in Ref. (3) were left out of consideration.

Processing of different XPS regions. The maximum of the Pt $4f_{7/2}$ peak is at about 71.15 eV, in good agreement with literature results (4). The effect of smoothing is negligible in the high-intensity Pt 4*f* region (Fig. 4). No characteristic differences are observed between the Pt peaks of the two samples, as is also shown by the difference spectrum in Fig. 4.

TABLE 2

X-Ray Diffraction Characterization of Pt-Black Catalyst Samples after Different Pretreatments

Sample	D (nm)[a]	α (%)[b]	σ (N/mm^2)[c]	ε_{111} (%)[d]	ε_{100} (%)[d]	d_X (%)[e]
Pt (as rec.)[f]	10.7	0.8	940	0.44	0.64	10.5
Pt-473	20.4	<0.1	154	0.07	0.10	5.5
Pt-633	29.1	<0.1	6	0	0	3.8

[a] Mean crystallite size.
[b] Mean stacking fault probability.
[c] Root mean square (r.m.s.) internal lattice stress.
[d] r.m.s. strain in ⟨111⟩ and ⟨100⟩ directions, respectively.
[e] X-ray dispersion, assuming spherical, or regular polyhedral particles (upper limit, due to aggregation of individual grains).
[f] Unsintered sample.

TABLE 3

Composition of Pt-633 and Pt-473 before and after Regeneration

Sample	Composition (atom%) O	K	C	Pt
Pt-633 (as received)				
XPS	19	0.5	47	33.5
AES	3	3	22	72
Regenerated				
XPS	19	1.5	27	52.5
AES	5	4	4	87
Pt-473 (as received)				
XPS	20	1	41	38
AES	2	2	22	74
Regenerated				
XPS	14	2	22.5	61.5
AES	3	5	5	87

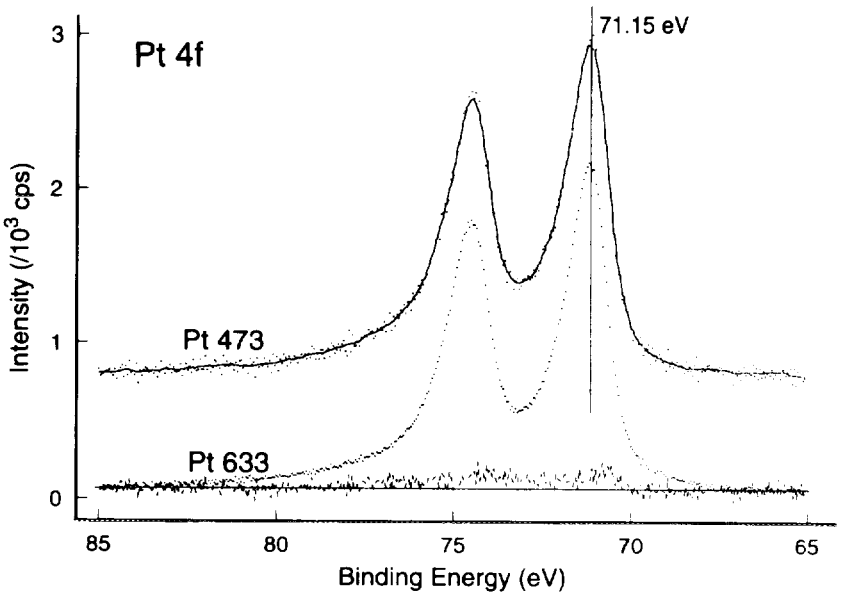

FIG. 4. Pt 4*f* XP spectra (200 scans, 20 ms each) of Pt-473 (shifted upwards) and Pt-633 in the as received state, after background subtraction (Shirley-type). Dots, unsmoothed spectrum; full line, smoothed spectrum. The bottom line is the difference spectrum, [(Pt-473)–(Pt-633)].

The atomic sensitivity of O 1*s* is lower; hence, they produced signals 5–10 times weaker than Pt and the spectra were more noisy. Figure 5 presents an example of two O 1*s* spectra with their line decomposition. The components were identified as PtO, OH, H_2O, and oxidized C, the respective binding energy (BE) values being around 530.3, 531.5, 532.5, and 533.8 eV. The highest BE component of O 1*s* (BE ca. 535.5 eV) was assigned to water clusters around K ions (23). An alternative assignment can be to inhomogeneously charged species, this component being present in a higher amount on Pt-633 as shown by electron flood gun experiments (6). The BE maxima agreed well with each other within a few tenths eV, and hence we attribute a physical reality to the individual components, with the reservations described under Experimental.

The difference spectrum [(Pt-473)–Pt-633)] for the as received state (Fig. 5b) indicates a positive peak at BE 530 eV, meaning an excess of PtO (an OH) in Pt-473, while the composite negative peaks at the higher (533–536 eV) BE regions point to an excess of water and oxidized carbon in Pt-633 before regeneration. The difference in the PtO and OH region disappears after regeneration (Fig. 5c), but Pt-633 still exhibits more oxygen in the H_2O and oxidized C regions.

A similar analysis of the C 1*s* band (Fig. 6) reveals low amounts of Pt-carbide in Pt-473 (uncertain, low intensity line at 283.3 eV). The components of the C 1*s* region identified as "C_xH_y polymer" (BE 284.5 eV) or "oxidized C" (BE 286.3 eV) represent respective sums of all sp^3-type hydrocarbons and those containing ether, alcoholic, or phenolic OH groups, while "graphite" (BE 285.5 eV) summarizes carbon in aromatic rings. The highest BE component (ca. 288 eV) was assigned to carbonylic or quinonic C=O groups. The difference spectrum [(Pt-473)–Pt-633)] before regeneration (Fig. 6b) reveals less graphite, more polymeric C_xH_y species, and oxidized carbon in Pt-633 than in Pt-473. The character of this difference is also preserved after regeneration (Fig. 6c). The possible asymmetry of the C 1*s* lines (24) has been neglected in this procedure.

The amount of each oxygen component is 1–7% of the total surface signal. The amount of minor C 1*s* components shows similar values but that of the major carbon components can reach 15–20% of the surface.

UPS. Figure 7 shows UP spectra of Pt-473 and Pt-633 recorded in the as received state and the difference of the two spectra [(Pt-473)–(Pt-633)] after normalizing their intensity at a BE value of 2.45 eV. A low intensity is observed at the Fermi edge in the as received state but the predominant feature is a high-intensity broad band between 6 and 10 eV, characteristic of surface carbon (25). A small positive peak appears in the difference spectrum at ca. 4 eV which may mean a C 2*p* intensity increase (26) in Pt-473, in agreement with its C excess in the graphite region (Fig. 6b). The higher intensity at ca. 6 eV in Pt-473 may originate from O^{2-} in PtO, in agreement with Fig. 5b. The C 1*s* excess in Pt-633 in the higher BE XPS region (Fig. 6b) may correspond to the higher UPS inten-

sity in the 7–14 eV region. Low-intensity water bands (ca. 6, 8, 12 eV) can be recognized in Pt-473.

Features due to oxygen-containing species are suppressed in the as received state but are abundant after regeneration where also the Fermi-edge intensity increases, corresponding to a higher fraction of exposed Pt surface. A difference spectrum constructed after normalizing the intensities of the UP spectra of the two regenerated samples (Fig. 8) shows no intensity differences between 0 and 3.5 eV (i.e., in the metallic intensity region) and a slightly higher intensity of Pt-633 in the range of impurities, OH (ca. 5.5 eV) and carbon (6.5–9 eV), the latter overlapping with water (6, 8, and 12 eV) present probably as a diffuse adsorbed layer. No sharp bands due to individual well-defined sorbed species such as OH and/or H_2O are seen.

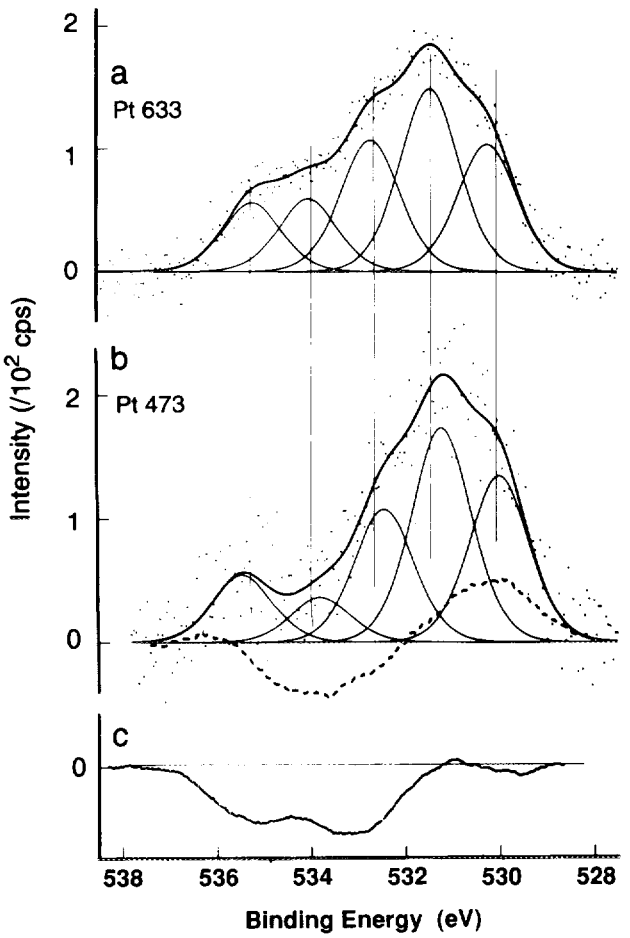

FIG. 5. O 1*s* region of the XP spectra of two Pt catalysts in their as received state, after Shirley-type background subtraction. (a) Pt-633, 1000 scans. The sum of the fitted components is shown together with the smoothed spectrum. (b) Pt-473, 405 scans. Dots denote unsmoothed spectra; full line, smoothed spectra and fitted components; dashed line, the difference spectrum in the as received state, i.e., [(Pt-473)–(Pt-633)]. (c) Difference spectrum [(Pt-473)–(Pt-633)] after regeneration (parent spectra not shown).

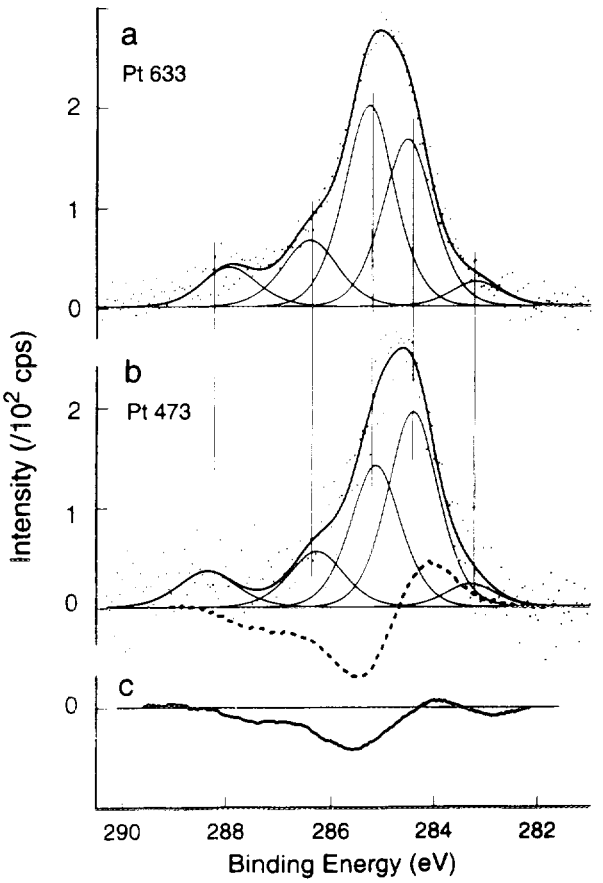

FIG. 6. C 1*s* region of the XP spectra of Pt-473 in as received state, after Shirley-type background subtraction. (a) Pt-633, 1000 scans. (b) Pt-473, 405 scans including the difference spectrum [(Pt-473)–(Pt-633)] in the as received state as a dashed line. (c) Difference spectrum [(Pt-473)–(Pt-633)] after regeneration (parent spectra not shown). Symbols and explanation, see Fig. 5.

DISCUSSION

There are definite differences between the catalytic properties of the two samples. Pt-633 produces more fragments and benzene, whereas the formation of saturated C_6 products (methylcyclopentane and even more isomers) prevail on Pt-473, which also has a slightly higher olefin selectivity. Although the actual selectivity values of these product classes are different, the hydrogen sensitivity and the shapes of the $S - X$ curves (Fig. 3) are similar with both Pt-blacks. Both catalysts show a marked response to the change of hydrogen pressure. Hydrogenolysis predominates at highest hydrogen excess ($H_2 : nH$ = 64 : 1.33), whereas olefin formation prevails at $H_2 : nH$ = 16 : 5.33. Benzene and isomers may be inherent primary products at low hydrogen excess.

As for hydrogenolysis characteristics, the *n*-hexane molecule splits predominantly at its middle C–C bond on supported (27) and unsupported (28) Pt catalysts. This is

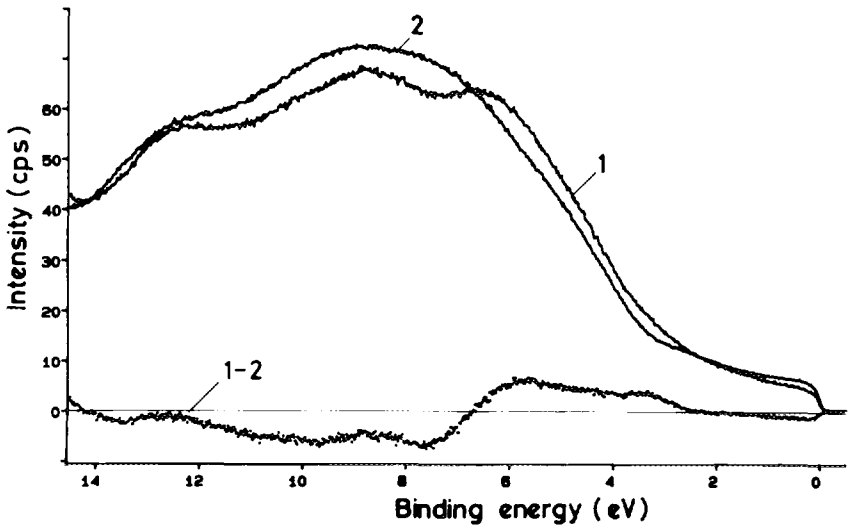

FIG. 7. He I UP spectra of Pt-473 (curve 1) and Pt-633 (curve 2) in the as received state normalized to each other at BE = 2.45 eV and their difference spectrum. Intensities: 10^3 cps.

also valid in our case, except for (a) the rather high ω_1 values at $p(n\mathrm{H}) : p(\mathrm{H_2}) = 1.33 : 16$ over Pt-633 (Table 1), and (b) the high percentage of methane at $p(nH) : p(\mathrm{H_2}) = 1.33 : 64$ (Table 1, last column), which does not change parallel to the ω_1 value. These deviations can be attributed (a) to a terminal splitting claimed to be favored on carbonized Pt sites (27, 29) that are present at low hydrogen excess, and (b) to a true multiple splitting (low M_f values, Table 1) at high hydrogen excess (27). The hydrogenolysis characteristics are less affected by hydrogen pressure changes on Pt-473 where fragmentation is less pronounced.

There are several possible interpretations for the likely reasons of the differences observed.

Structure sensitivity. This well-known possibility (30) was used earlier as one of the possible explanations for results obtained with different Pt samples (3, 31). Three-atom ensembles of sixfold symmetry were assumed to promote aromatization on dispersed alloy catalysts (32). Single Pt atoms were found to be sufficient for propane dehydrogenation to propene (33). Two-atom ensembles may be sufficient for the common C_5-cyclic surface intermediate of isomerization and C_5cyclization (34), espe-

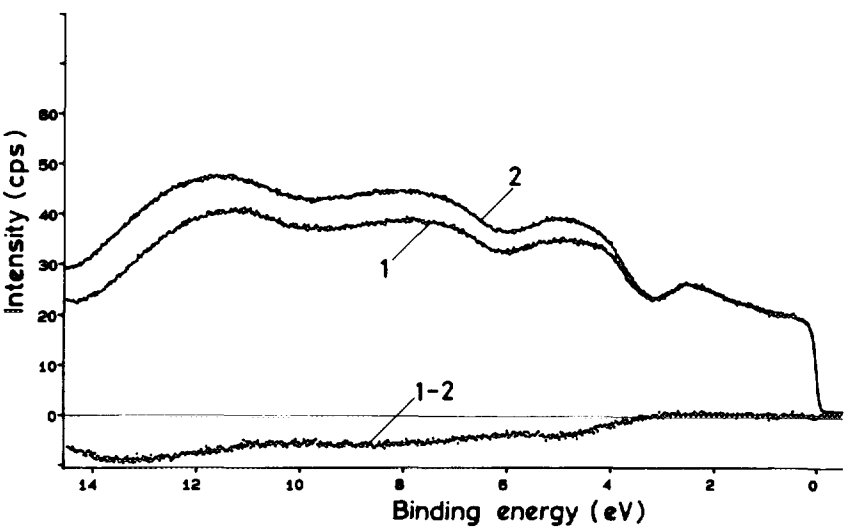

FIG. 8. He I UP spectra of regenerated Pt-473 (curve 1) and Pt-633 (curve 2) and their difference spectrum. Intensities: 10^3 cps.

cially if we assume dehydrogenation to a minimum degree (35). Single-crystal studies indeed confirmed that planes of hexagonal symmetry had enhanced activity in benzene formation from *n*-hexane, while kinks and edges of analogous symmetry were even more active (36). The electron micrographs (3) showed rounded and irregular crystallites in both catalysts (with no predominance of any definite Miller index plane). X-ray diffraction, however, shows no lattice strain with Pt-633. Its larger crystallites can expose a higher amount of low(er) Miller index planes of sixfold symmetry that may be responsible for the higher aromatization activity. At the same time, the rounded surfaces may contain a number of kink and edge sites (37). Their effect may be twofold: sixfold symmetry sites may promote benzene formation and these "ledge structures" may also enhance hydrogenolysis (38). A methylcyclopentane ring opening showed a lower structure-sensitivity over single crystal planes (39). The two-atom ensembles assumed for this process (31, 40) may be more abundant on the smaller crystallites of Pt-473 (Table 2).

Surface purity. Here the possible effects of overall concentration of detected C or O impurities should be considered (7). Their firm attachment to Pt is shown by fragments such as PtO^- and $PtC_2H_x^+$ in SIMS (22). No dramatic differences can be seen in the surface compositions (Tables 4 and 5); nevertheless, Pt-633 contains slightly more O and C. The similarity of the Fermi-edge region of the UP spectra after regeneration with slightly more overlayer-type signal in Pt-633 (Fig. 8) confirms that both catalysts have sufficient free metallic sites for catalytic reactions.

A further possibility of impurity effects arises from "adsorption sites" and "reactive sites" being different (38). A similar *amount* of impurity in various *positions* on crystallites (having themselves different dispersion and geometry) may give rise to a quite different "traffic" of adspecies between these two types of surface centers.

The chemical state, stability, and physical form of impurities. The majority of carbon has been assumed to form three-dimensional overlayers (5, 6, 41). The different catalytic effect of carbonaceous deposits in various chemical form and position on different catalysts has been reviewed (42). The amount of individual carbon components is different in the two catalysts. No Pt–C can be detected after regeneration over Pt-473 as opposed to Pt-633. Pt–C ensembles have been claimed to be responsible for terminal splitting (29) as well as for olefin formation (27) and this agrees well with the catalytic properties of Pt-633. Carbon accumulation influenced the selectivity of propylcyclobutane ring opening markedly (43). In our view, Pt–C may mean hydrocarbon fragments consisting of one or more C atoms attached by chemical bonds to

TABLE 4

Residual Percentage of Carbon and Oxygen after Regeneration as Determined by XPS[a]

	Catalyst	
	Pt-633	Pt-473
(A) O 1s[b]	~98	~70
Total		
530.5 (PtO)		
531.4 (OH)		
532.5 (H_2O)	~98	~70
533.8 (ox. C)		
535.2 (charged)		
(B) C 1s[b]		
Total	~60	~50
283.3 (PtC)	~80	0
284.5 (graphite)	~50	~50
285.5 (C_xH_y)	~50	~50
286.3 (ox. C)	~90	~100
ca. 288 (C=O; COOH)	~100	~150

[a] In percentages of the surface concentration in the sample without regeneration. Fitting to smoothed spectra with the DS-100 software was used for both calculations.

[b] Components indicated by BE values in eV.

TABLE 5

Ratios Isomers/Methylcyclopentane

Catalyst	$p(H_2)$ (kPa)	$p(n\text{H})$ (kPa)	Isomer/MCP at approximate conversion (%) 5	10	15	Ref.
Present study						
Pt-633	16	1.33	0.9	1.0	1.0	
	64	1.33	1.8	2.3	2.8	
Pt-473	16	1.33	0.8	0.9	1.2	
	64	1.33	3.7	5.0	—	
Literature data						
"Fresh" Pt-473[a]	16	1.33	2.5	3.3	—	(10)
"Used" Pt-473[b]	16	1.33	1.3	1.2	1.2	(10)
	64	1.33	2.2	2.8	3.7	(10)
Pt–IV[c]	16	1.33	0.8	0.8	0.9	(11)
	64	1.33	4.3	4.5	—	(11)
Pt–IV/K[d]	16	1.33	0.7	0.8	0.8	(11)
	64	1.33	3.7	4.2	4.8	(11)

[a] Catalyst reduced with HCHO, presintered at 473 K; the very first runs in the catalyst life (10).

[b] As under [a], but in a later stage of the catalyst life.

[c] Catalyst reduced with hydrazine, containing practically no K, (Pt/IV) corresponds to the labeling used in Ref. (11).

[d] The same catalyst as under [c], KOH added (ca. 0.6% K).

Pt rather than a contiguous platinum carbide phase. These entities dehydrogenate upon evacuation (44), which was the customary termination of the catalytic run, and seem to be rather unstable also upon exposure to air. Therefore, their actual amount during reaction should be higher than that detected by XPS. The higher amount of graphite observed in Pt-473 may probably be aggregated and represents a more inert carbon type from the catalytic point of view.

Even though the actual concentration of the individual carbon components should be handled with caution, there is no doubt that various areas of the C 1*s* band do not respond uniformly to regeneration (Table 4). The O_2–H_2 treatment at 600 K removed Pt–C entirely from Pt-473, while about 80% of it remains in Pt-633. The amount of remaining graphite and hydrocarbonaceous polymers is around 50% in both catalysts. Hardly any oxidized C is removed from either sample, while regeneration even increases the amount of highest BE carbon species (carbonate/carboxylic C) in Pt-633. When evaluating these results, one must remember that during regeneration (i) smaller carbonaceous molecules tend to aggregate to give larger islands and (ii) some three-dimensional deposits undergo partial oxidation to give oxidized graphite or a $C_xH_yO_n$ polymer. These latter entities may have been responsible for the enhanced selectivity of ring opening of methylcyclopentane in the vicinity of the methyl substituent (45).

Quinonic C=O groups were detected in the latter species (46). The interaction between Pt and quinonic C=O groups of a carbon support caused a shift of the Pt 4f BE toward higher values (47). The detection limit of this shift was ca. 0.7 eV and corresponded to a surface concentration of C=O groups of 15%. Our catalyst corresponds to the reverse case, containing "carbon on a Pt support" and the amount of C=O entities is not higher than a few percentages. Hence, the minor differences (0.1–0.2 eV) in the Pt 4*f* BE values of Pt-633 and Pt-473 cannot be attributed with any certainty to such an interaction.

Any possible surface CO with BE between 256 and 287 eV (48) overlaps with the two highest BE components of the C 1*s* line. Carbonate, above all as potassium carbonate, should appear above 289 eV (49). The broad peaks of overlayer-like surface species prevent detection by UPS of any possible adsorbed CO at ca. 9 and 11.5 eV both before and after regeneration (Figs. 7 and 8).

Hardly any oxygen is removed from Pt-633, while regeneration leaves ca. 70% of the original O content on Pt-473 (Table 4). One has to remember that O_2–H_2 treatments under more severe conditions could even increase the amount of oxygen (as PtO, BE ca. 530 eV) in Pt-633 (5, 6). The presence of surface oxygenates at the very beginning of the run was concomitant with the occurrence of multiple hydrogenolysis (6). An enhanced hydrogenolysis was indeed observed at the beginning of the runs (Figs. 1 and 3). These sorbed OH/H_2O species are replaced within a few minutes by not-too-deeply dehydrogenated sorbed hydrocarbons and the catalytic propensities become stabilized. The initial high hydrogenolysis is less pronounced with the Pt-473 sample where the amount of residual oxygen was lower (Table 4). It is difficult to decide whether surface oxygenates are "spectator species" or active participants in the initial hydrogenolysis reaction. This process was promoted by ample amounts of surface hydrogen after regeneration (50). Surface OH and H_2O entities were rather stable on Pt films; upon heating they gave off hydrogen (51) and their hydrogen content may belong to the general surface hydrogen pool.

Hydrogen effects. Hydrogen may control the amount and/or the degree of dehydrogenation of the **reactive** surface intermediates (31, 52, 53). Aromatization was attributed to a more deeply dehydrogenated surface intermediate, while a less dehydrogenated one may be responsible for C_5-cyclic reactions (35, 40). A higher available hydrogen concentration on Pt-473 may be the reason why this catalyst produces more C_6 saturated products (Fig. 3). This may be connected with its detectable strain and somewhat higher lattice anisotropy (Table 2) accommodating more hydrogen in subsurface areas, crevices, grain boundaries, or less perfect crystal regions (54). Alternatively, hydrogen could control the amount and state of **nonreactive** hydrocarbonaceous deposits [see also Ref. (10)], and by doing so, the abundance of free and partly hydrocarbon-covered surface sites (29, 55). Indeed, a higher Pt intensity of Pt-473 in XPS indicates a higher amount of surface Pt sites (Table 3), although no difference is seen between the two samples as far as the metallic Pt UPS intensity from the uncovered Pt fraction is concerned (Fig. 8).

Isomer/MCP ratio as a diagnostic tool on the surface state of Pt. The formation of isomers from the common C_5-cyclic intermediate needs the uptake of two hydrogen atoms and hence should be more favored than C_5-cyclization if much hydrogen is available. "MCP_s" can be formed even on "adsorption" sites, as evidenced by hydrogenative desorption experiments following *n*-hexane adsorption (53) or reaction (57) on various Pt catalysts. parallel to these skeletal reactions, a proportion of surface species gradually lose their hydrogen atoms and remain on the surface. In single-pass reactors, the constant renewal of the surface under hydrogen can lead to increasing amounts of isomers as the reaction proceeds (59). In our closed loop, however, recirculated olefins readsorb as indicated by Figs. 1–3 and form "unsaturated surface species." They may have a C_5-cyclic structure when they are produced by

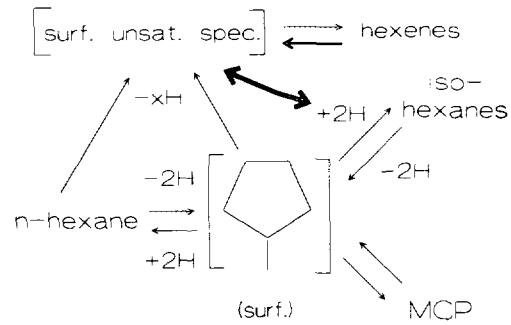

FIG. 9. A simplified scheme for the formation of C_6 saturated products and hexenes from *n*-hexane. The thick arrow with two heads denotes a competition of hydrogen and unsaturated hydrocarbon residues (which may or may not have a C_5-cyclic structure) for the same surface sites.

the dehydrogenation of MCP_s. The scheme in Fig. 9 has been constructed on the basis of the kinetic scheme (58), taking into account their accumulation.

The ratio isomer/MCP can, therefore, be used to characterize the hydrogen availability on a given active surface (56). This ratio was "frozen" at lower $p(n\mathrm{H})/p(\mathrm{H_2})$ values, while real differences manifested themselves at highest hydrogen excess (Table 5). Under these conditions, not only were more isomers produced but their amount also increased during the run, as expected on earlier kinetic considerations (58, 59). Comparing several Pt-blacks indicates that this ratio is a sensitive probe of the catalyst purity. Pt-473 gave, as a rule, higher values of the isomer/MCP ratio than Pt-633. A Pt-473 sample prepared in the same way produced a higher isomer/MCP ratio; after a number of runs ("used Pt") the values approached those observed with the present Pt-473 (10). A K-free catalyst (Pt/IV) showed high isomer excess, but adding K decreased this ratio (11).

Hydrogen competes with hydrocarbon reactants for reactive surface sites, resulting in bell-shaped curves of yields as a function of $p(\mathrm{H_2})$ (3, 6–12). This is more pronounced with Pt-633 (3) where XPS shows higher amounts of oxidized carbon, its amount even increasing after regeneration (Table 4). Carbonyl groups in carbonaceous deposits have been shown to participate in hydrogen transfer reactions (46). Such groups in the vicinity of Pt sites may serve as "hydrogen catchers." An increase of hydrogen pressure would hydrogenate these carbonyl groups rather than creating hydrogen-rich active sites for hydrocarbon reactions.

We believe that physical catalyst characterization methods can supply useful information for the possible active sites of the catalyst. Since, however, the actual activity is mainly determined by atomically disperse structures, their limitations have to be kept in mind and their results should be combined with the information supplied by the catalytic reactions of probe molecules.

ACKNOWLEDGMENTS

Z. P. thanks Professor G. Ertl for an invitation to an extended stay in Berlin at the Fritz-Haber-Institut (subsidized by the Max-Planck-Gesellschaft) during which the electron spectroscopic measurements were carried out. The catalytic runs were carried out in Budapest; this activity and additional spectrum evaluation in Berlin were also supported financially by the National Science Foundation (OTKA Grants 1309 and 1887).

REFERENCES

1. Baird, T., Paál, Z., and Thomson, S. J., *J. Chem. Soc., Faraday Trans. 1* **69,** 50 (1973); **69,** 1237 (1973).
2. Manninger, I., Paál, Z., and Tétényi, P., *Z. Phys. Chem., Neue Folge* **132,** 193 (1982); *Z. Phys. Chem., Neue Folge* **143,** 247 (1985).
3. Paál, Z., Zimmer, H., Günter, J. R., Schlögl, R., and Muhler, M., *J. Catal.* **119,** 146 (1989).
4. Paál, Z., Tétényi, P., Prigge, D., Wang, X. Zh, and Ertl, G., *Appl. Surf. Sci.* **14,** 307 (1982–83).
5. Paál, Z., Schlögl, R., and Ertl, G., *J. Chem. Soc. Faraday Trans.* **88,** 1179 (1992).
6. Paál, Z., Schlögl, R., and Ertl, G., *Catal. Lett.* **12,** 331 (1992).
7. Paál, Z., and Schlögl, R., *Surf. Interface Anal.* **19,** 524 (1992).
8. Paál, Z., Zimmer, H., and Günter, J. R., *Z. Phys. Chem., Neue Folge* **164,** 1135 (1989).
9. Paál, Z., Zimmer, H., and Matusek, K., *J. Catal.* **141,** 648 (1993).
10. Paál, Z., and Zhan, Zh., in preparation.
11. Paál, Z., Zhan, Zh., Fülöp, E., and Tesche, B., submitted for publication.
12. Paál, Z., Groeneweg, H., and Zimmer, H., *Catal. Today* **5,** 199 (1989).
13. Paál, Z., Räth, M., Zhan, Zh., and Gombler, W., *J. Catal.* **147,** 342 (1994).
14. Vogel, W., Tesche, B., and Schulze, W., *Chem. Phys.* **74,** 137 (1983).
15. Vogel, W., *J. Catal.* **121,** 356 (1990).
16. Davis, L. E., MacDonald, N. C., Palmberg, P. W., Riach, G. E., and Weber, R. E., "Handbook of Auger Electron Spectroscopy," Physical Electronics, 1976.
17. Abbot, J., Corma, A., and Wojciechowski, B. W., *J. Catal.* **92,** 398 (1985).
18. Margitfalvi, J., Szedlacsek, P., Hegedüs, M., and Nagy, F., *Appl. Catal.* **15,** 69 (1985).
19. Paál, Z., and Tétényi, P., *Nature* **267,** 234 (1977).
20. Ponec, V., and Sachtler, W. M. H., Proceedings, 5th International Congress on Catalysis, Palm Beach, 1972," (J. W. Hightower, Ed.), Vol. 1, p. 645. North-Holland, Amsterdam, 1973.
21. Leclercq, G., Leclercq, L., and Maurel, R., *J. Catal.* **50,** 87 (1977).
22. Paál, Z., and Marton, D., *Appl. Surf. Sci.* **26,** 161 (1986).
23. Bonzel, H. P., Pirug, G., and Winkler, A., *Surf. Sci.* **175,** 287 (1986).
24. Schlögl, R., *Surf. Sci.* **189/190,** 861 (1987); Schlögl, R., and Boehm, H. P., *Carbon* **21,** 45 (1983).
25. Evans, S., and Thomas, J. M., *Proc. R. Soc. London A* **353,** 103 (1977).
26. Atkinson, S. J., Brundle, C. R., and Roberts, M. W., *Faraday Discuss. Chem. Soc.* **58,** 62 (1974).
27. Paál, Z., Groeneweg, H., and Paál-Lukács, J., *J. Chem. Soc., Faraday Trans.* **86,** 3159 (1990).
28. Zimmer, H., Dobrovolszky, M., Tétényi, P., and Paál, Z., *J. Phys. Chem.* **90,** 4758 (1986).
29. Ponec, V., *in* "Advances in Catalysis" (H. Pines, D. D. Eley, and P. B. Weisz, Eds.), Vol. 32, p. 149. Academic Press, New York, 1983.

30. Boudart, M., *in* "Advances in Catalysis" (H. Pines, D. D. Eley, and P. B. Weisz, Eds.), Vol. 20, p. 153. Academic Press, New York, 1969.
31. Paál, Z., *Catal. Today* **12,** 297 (1992).
32. Biloen, P., Helle, J. N., Verbeek, H., Dautzenberg, F. M., and Sachtler, W. M. H., *J. Catal.* **63,** 112 (1980).
33. Biloen, P., Dautzenberg, F. M., and Sachtler, W. M. H., *J. Catal.* **50,** 77 (1977).
34. Barron, Y., Maire, G., Muller, J. M., and Gault, F. G., *J. Catal.* **5,** 428 (1966).
35. Finlayson, O., Clarke, J. K. A., and Rooney, J. J., *J. Chem. Soc., Faraday Trans. 1* **80,** 191 (1984).
36. Davis, S. M., Zaera, F., and Somorjai, G. A., *J. Catal.* **85,** 206 (1984).
37. Rounded crystallites may be analogous to a field emission tip for which a ball-model structure is depicted by G. Ehrlich, *in* "Advances in Catalysis" (H. Pines, D. D. Eley, and P. B. Weisz, Eds.), Vol. 14, p. 314. Academic Press, New York, 1983.
38. Dauscher, A., Garin, F., and Maire, G., *J. Catal.* **105,** 233 (1987).
39. Zaera, F., Godbey, D., and Somorjai, G. A., *J. Catal.* **101,** 73 (1986).
40. Paál, Z., *in* "Advances in Catalysis" (H. Pines, D. D. Eley, and P. B. Weisz, Eds.) Vol. 29, p. 273. Academic Press, New York, 1980.
41. Somorjai, G. A., and Zaera, F., *J. Phys. Chem.* **86,** 3070 (1982).
42. Menon, P. G., *J. Mol. Catal.* **59,** 207 (1990).
43. Török, B., Molnár, A., Pálinkó, I., and Bartók, M., *J. Catal.* **145,** 295 (1994).
44. Garin, F., Maire, G., Zyade, S., Zauwen, M., Frennet, A., and Zielinski, P., *J. Mol. Catal.* **58,** 185 (1990).
45. Paál, Z., *J. Mol. Catal.*, **94,** 225 (1994).
46. Schraut, A., Emig, G., and Sockel, H.-G., *Appl. Catal.* **29,** 311 (1987).
47. Antonucci, P. L., Alderucci, V., Giordano, N., Cocke, D. L., and Kim, H., *J. Appl. Electrochem.* **24,** 58 (1994).
48. Kiskinova, M., Pirug, G., and Bonzel, H., *Surf. Sci.* **133,** 321 (1983).
49. Rehren, C., Muhler, M., Bao, X., Schlögl, R., and Ertl, G., *Z. Phys. Chem.*, **174,** 11 (1991).
50. Sárkány, A., *Catal. Today* **5,** 173 (1989).
51. Akhtar, M., and Tompkins, F. C., *Trans Faraday Soc.* **67,** 2454 (1971); Akhtar, M., and Tompkins, F. C., *Trans Faraday Soc.* **67,** 2461 (1971).
52. Paál, Z., Székely, G., and Tétényi, P., *J. Catal.* **58,** 108 (1979).
53. Foger, K., and Gruber, H. L., *J. Catal.* **122,** 307 (1990).
54. Wells, P. B., *J. Catal.* **52,** 498 (1978).
55. Sárkány, A., *J. Chem. Soc., Faraday Trans. 1* **85,** 1523 (1989).
56. Paál, Z., *in* "Hydrogen Effects in Catalysis" (Z. Paál and P. G. Menon, Eds.), p. 449. Dekker, New York, 1988.
57. Sárkány, A., *J. Chem. Soc., Faraday Trans. 1* **84,** 2267 (1988).
58. Amir-Ebrahimi, V., and Gault, F. G., *J. Chem. Soc., Faraday Trans. 1* **76,** 1735 (1980).
59. Chow, M., and McVicker, G. B., *J. Catal.* **112,** 290 (1988).